Thiolate-Capped Silver Nanoparticles: Discerning Direct Grafting from Sulfidation at the Metal–Ligand Interface by Interrogating the Sulfur Atom

Marianne Marchioni, Chiara Battocchio, Yves Joly, Christelle Gateau, Silvia Nappini, Igor Pis, Pascale Delangle, Isabelle Michaud-Soret, Aurélien Deniaud, Giulia Veronesi

Thiolate-capped silver nanoparticles: discerning direct grafting from sulfidation at the metal-ligand interface by interrogating the sulfur atom

Marianne Marchioni[a], Chiara Battocchio[b], Yves Joly[c], Christelle Gateau,[e] Silvia Nappini[d], Igor Pis[d,e], Pascale Delangle[f], Isabelle Michaud-Soret[a], Aurélien Deniaud[a], Giulia Veronesi[a,g,*]

[a] Univ. Grenoble Alpes, CNRS, CEA, IRIG, Laboratory of Chemistry and Biology of Metals, 38000 Grenoble, France

[b] Univ. Roma Tre, Dept. of Sciences, Via della Vasca Navale 79, 00146 Rome, Italy

[c] University Grenoble Alpes, CNRS, Grenoble INP, Institut Néel, 38000 Grenoble, France.

[d] Consiglio Nazionale delle Ricerche (CNR) Istituto Officina dei Materiali (IOM), Laboratorio TASC in Area Science Park S.S. 14 km 163.5 34149 Trieste, Italy

[e] Elettra-Sincrotrone Trieste S.C.p.A, S.S. 14, km 163.5, 34149 Basovizza, Trieste, Italy

[f] Univ. Grenoble Alpes, CEA, CNRS, IRIG, SYMMES, 38000 Grenoble, France

[g] ESRF, The European Synchrotron, 71 Avenue des Martyrs, 38000 Grenoble, France

Abstract

Grafting thiol-bearing molecules at the surface of silver nanoparticles (AgNPs) is a successful strategy to tune their optical and antibacterial properties. The capping layer generated from self-assembly of the ligands at the nanoparticle surface determines the range of possible applications of the resulting material. In particular, direct grafting of the thiol heads to surface Ag(I) can occur, with various hybridizations of the S atom, sp versus sp^3. Alternatively, a passivating Ag_2S layer can form. We make use of S K-edge X-ray Absorption Near Edge Structure (XANES) and synchrotron-based X-ray Photoelectron Spectroscopy (XPS) to probe the metal-ligand interface in different thiol-capped AgNPs. The use of cryogenic conditions for XAS analyses reveals a peculiar spectral signature for thiolates chemisorbed on the AgNPs surface, unambiguously distinguished from that of Ag_2S. *Ab initio* simulations of XANES spectra and XPS analyses are used to predict the grafting mode, suggesting that different ligand architectures promote slightly different proportions of sp/sp^3 sites, and a dramatic variability in the stability of the nanomaterial that can evolve toward either self-assembly or dissolution of the AgNPs.

INTRODUCTION

Self-assembling of thiolates on planar metal surfaces generates self-assembled-monolayers (SAMs), which are used as building blocks of technological devices since four decades.[1,2] More recently, the concept of self-assembling has been extended to nanoparticles (NPs) surfaces, where thiolate capping agents play the multifold role of protection, functionalization and control of the physicochemical properties of the metallic core.[3] SAMs formation is highly efficient on silver nanoparticles (AgNPs), because of the high affinity of the thiolate heads for the Ag(I) surface atoms of the NPs. Therefore, capping AgNPs with thiol-bearing molecules is a widespread strategy to tune their optical and antibacterial properties.[4–7]

The antibacterial action of AgNPs is due to their dissolution and release of Ag(I) ions, which are toxic for bacteria.[8,9] Considering that their use as biocides in consumer products and medical devices entails human exposure, it is desirable to tune Ag(I) release to the minimum amount necessary to kill bacteria, in order to avoid side effects and resistance phenomena, and to improve resource efficiency.[10] To this end, thiol-bearing capping agents can help to control ion release, thus to modulate the antibacterial properties of AgNPs.[11–13]

Depending on the thiol-bearing molecules and on the synthesis protocol, thiolates can either graft directly to the AgNPs surface,[6,12,14] or form a core@shell material exhibiting an intermediate layer of silver sulfide (Ag_2S).[15,16] The formation of such layer, also called sulfidation, passivates the NPs preventing ion release, resulting in functionalized stable materials used for their optical properties,[17] but not efficient as biocides. Sulfidation is a well-known environmental transformation of AgNPs that weakens their ecotoxicology hazard.[18,19]

In contrast, when thiolates graft directly to the AgNPs surfaces, ion release is still possible, and the final material exhibits a biocidal activity.[12,20] In this context, we recently proposed a biocide material made of AgNPs coated by the three-thiol bioinspired ligand $\mathbf{L^{3S}}$ that mimics the biological binding site of Cu(I) in metallothioneins.[21] This ligand also forms complexes with Ag(I), where the metal binds three S atoms in trigonal coordination.[22] When interacting with AgNPs, $\mathbf{L^{3S}}$ promotes the formation of size-controlled assemblies of NPs, which proved to efficiently release Ag(I). The biocidal activity of AgNPs assemblies was measured on different bacterial strains.[12]

It must also be considered that not all thiol-bearing molecules graft to AgNPs surfaces: depending on the ligand and on its concentration, thiols can foster AgNP dissolution and Ag(I) release in solution over time, resulting in unstable systems.[23] We demonstrated that the number of thiol functions in the ligand, as well as their orientation, influence the dissolution rate.[24] This has implications in bio-medicine, since the main transformation of AgNPs in cells, which are thiol-rich environments, is dissolution followed by the formation of molecular Ag(I)-thiolate complexes that impair the cell functions.[25–27]

The above-mentioned considerations, which take into account the interaction between thiol-bearing molecules and AgNPs in a transversal approach spanning from nanotechnology to biology, highlight the importance of the surface phenomena at the thiol-metal interface in the determination of the stability and properties of the system. In particular, the occurrence of sulfidation or of direct chemisorption on the NPs surface will influence the range of possible applications of the nanomaterial.

Probing the thiol-metal interface is crucial for the characterization of engineered nanomaterials, nevertheless it is experimentally challenging. Several Density Functional Theory (DFT) studies predict computationally the grafting mode of thiolates on flat silver surfaces and small Ag clusters.[2,3,14,28] From the experimental point of view, Scanning Tunneling Microscopy (STM) allows to assess the electrical properties of coated NPs,[29] whereas X-ray Photoelectron spectroscopy (XPS) is the technique of choice for the interrogation of the grafting mode of the capping agent.[6,12,16] Sulfur K-edge X-ray Absorption Spectroscopy (XAS) has been sporadically used to determine the chemistry of sulfur atoms grafted to metallic NPs.[15,16,30]

In this work, we make use of S K-edge XAS, more specifically of the analysis of the near-edge spectral region (XANES, for X-ray Absorption Spectroscopy Near Edge Structure) and of Synchrotron Radiation X-ray Photoelectron Spectroscopy (SR-XPS) to interrogate selectively the metal-ligand interface in different AgNPs-thiolate systems as stable engineered nanomaterials and unstable colloidal suspensions, in which the NPs dissolve over time. We provide a robust set of XANES reference compounds that allows for the discrimination between direct surface binding and formation of an $Ag@Ag_2S$ core@shell structure. We performed XAS experiments on frozen solutions of AgNPs-thiolate systems, which brought us to revisit previous literature in the light of preparation artifacts. The possibility to dissect the fine details of thiol-metal binding opens new perspectives for the characterization of engineered nanomaterials and for the control of their physicochemical properties.

METHODS

Sample preparation. Citrate-stabilized, 20 nm diameter AgNPs were synthesized based on a reported protocol.[31] Briefly, $AgNO_3$ was reacted with tannic acid in the presence of citrate. An aqueous solution (100 mL) containing 2 mM sodium citrate and 50 nM tannic acid were heated at 90 °C under 800 rpm stirring. When this temperature was reached, five sequential additions of $AgNO_3$ (200 µL) at 25 mM were done every 5 min. Upon AgNP synthesis, the solution becomes yellow. AgNPs are finally recovered by 1 hour centrifugation at 9000 g. The pellet containing AgNPs was washed twice with an aqueous solution of 2 mM sodium citrate.

The $\mathbf{L^{3S}}$ ligand was synthesized and characterized as previously described.[21] 10 mM $\mathbf{L^{3S}}$ in 10 mM HEPES pH 7.5 buffer/Acetonitrile (6/4) is used for the preparation of AgNPs assemblies. Assemblies were prepared, purified, and characterized as previously described.[12] The original buffer (10 mM HEPES, 2 mM sodium citrate pH 7) was replaced by 2 mM citrate, pH 7.4, to avoid having S from the sulfonate moiety of HEPES in the buffer. The assemblies were purified on a sucrose gradient and rinsed 3 times by centrifugation in citrate buffer, in order to remove HEPES from the $\mathbf{L^{3S}}$ stock solution. The structural and optical properties of the assemblies in 2 mM citrate buffer were unchanged with respect to the previously reported properties.[12]

The other thiol-bearing molecules were purchased: GSH from Sigma-Aldrich, PC6 from Eurogentec. For both XAS and XPS, NP-containing solutions were prepared in Na-citrate 2 mM buffer. Ag(I) complexes were formed in solution in Tris buffer at pH 7.4 by adding thiol molecules and $AgNO_3$ (Sigma Aldrich) in Ag:S = 1:1 ratio. The same Ag:S = 1:1 ratio was used for AgNPs-thiol and Ag(I)-thiol solutions.

XANES data collection and analysis. S K-edge XANES spectra were collected on the beamline ID21 of the ESRF.[32] A Si mirror allowed for harmonic rejection. Without the use of

focusing optics, the beam size was determined by the diode used to measure the incoming current. The beam size at sample was 350 µm in diameter, and the incoming flux $7.8 \cdot 10^{10}$ photons/s. In concentrated solutions, to avoid the saturation of the detector, a 200 µm pinhole was used and provided a flux at sample of $3.5 \cdot 10^{10}$ photons/s. All samples were prepared and frozen in a glove box and analyzed at the temperature of 110 K in the LN_2 –cooled cryostat of ID21. A 2 µl drop of each sample solution was sandwiched between two Ultralene (SPEX SamplePrep) foils, frozen and clamped in the Cu sample holder. The S absorption edge was scanned in the 2460 – 2540 eV energy range with 0.25 eV steps, with a Si(111) double crystal monochromator ($\Delta E/E \sim 2 \times 10^{-4}$). The energy scale was calibrated by setting the peak position of the GSH sample at 2473.7 eV. The emitted fluorescence signal was detected with an energy-dispersive, large area (80 mm^2) SDD detector equipped with a Be window (XFlash SGX from RaySpec). In order to avoid beam-induced damage, individual scans with a dwell time of 0.1 s per energy point were acquired (scan duration: 32 s). Different spots on the sample drop were probed and their spectra were summed up in order to provide a total integration time of 1 to 6 s per energy point. The Athena software was used to normalize XANES spectra with standard methods and to perform linear combination fitting analysis.[33]

***Ab initio* XANES simulations.** S K-edge XANES spectra were simulated with the FDMNES software,[34] making use of the finite difference method to solve the relativistic Schrödinger equation,[35,36] including the spin-orbit interaction. Spin-orbit cannot be neglected in systems with relatively heavy atoms such as Ag. The finite difference method is also important because it uses a free shape potential, which is mandatory in these no dense and low symmetry systems. The calculation of the XANES spectra needs first a self-consistent calculation to obtain the electronic structure. Both steps of the calculation are done in cluster of atoms centered on the absorbing one. We found that a 5.2 Å cluster radius was necessary to get satisfactory results. Within this radius, the cluster contains the Cys moiety, as well as Ag atoms from the NP surface and two more atomic layers below the Ag (111) surface. The crystal structure of Cys from the CSD[37] entry LCYSTN04 was used as input structure for all calculations, without ever modifying its geometry. Additional information about the choice of the simulation parameters is provided as Supplementary Information.

Synchrotron Radiation X-ray Photoelectron Spectroscopy. SR-XPS experiments were performed on the beamline BACH of the ELETTRA synchrotron (Basovizza, IT).[38] The XPS data were collected using a hemispherical electron energy analyzer (Scienta R3000, pass energy 50 eV, angular mode) at an angle of 60° with respect to the X-ray incidence direction. The spectra were recorded at emission angle 60° from the surface normal, with light linearly polarized in the horizontal plane. The energy resolution was determined by measuring the width of the Fermi edge on a gold reference sample at a given incident photon energy. For all samples we acquired C 1s, Ag 3d, O 1s, and N 1s core-level spectra with 596 eV photon energy (PE), C 1s and S 2p core levels with 380 eV PE, and the total binding energy resolution was 0.3 and 0.2 eV, respectively. Solutions (~ 20 µl) were deposited on Si(111) or Au-coated Si wafers and dried at room temperature. The buffer solution for all samples was 2 mM Na-citrate, which was initially characterized. Photoemission signal from the substrate was strongly attenuated thanks to the low photon energies and to the experimental geometry. All binding energies were referenced to the aliphatic C 1s peak at 285.0 eV. The C 1s core level spectrum of the buffer was used in data analysis to derive the width of the Voigt components used to reproduce the experimental data. S 2p core level spectra were decomposed into Voigt doublets, fixing the

ratio of the two spin-orbit components ($S2p_{3/2}/S2p_{1/2}$=2/1) and their energy separation (1.2 eV). Spectral deconvolution was performed with the KolXPD program,[39] using Voigt functions to reproduce the spectral contributions. The curve width was constrained to the same value for all functions of the same core-level signal. The experimental resolution was monitored over the experiment by measuring the full width half maximum (FWHM) of the Au 4f signal; the measured value was 0.59 eV for all spectra collected during the experiment, confirming the resolution and the stability of the experimental setup. The FWHM of the C 1s spectra, measured on the buffer solution and kept constant in all the following fits, was 1.11 eV.

RESULTS AND DISCUSSION

S K-edge X-ray Absorption Spectroscopy. In order to shed light on the interactions between thiolates and AgNPs surfaces, we acquired S K-edge XAS spectra of different thiolate-AgNPs solutions and model sulfur compounds in cryogenic conditions. A schematic representation of all thiol-bearing molecules used in this study is given in Scheme 1.

Scheme 1. Thiol-bearing molecules used in this study.

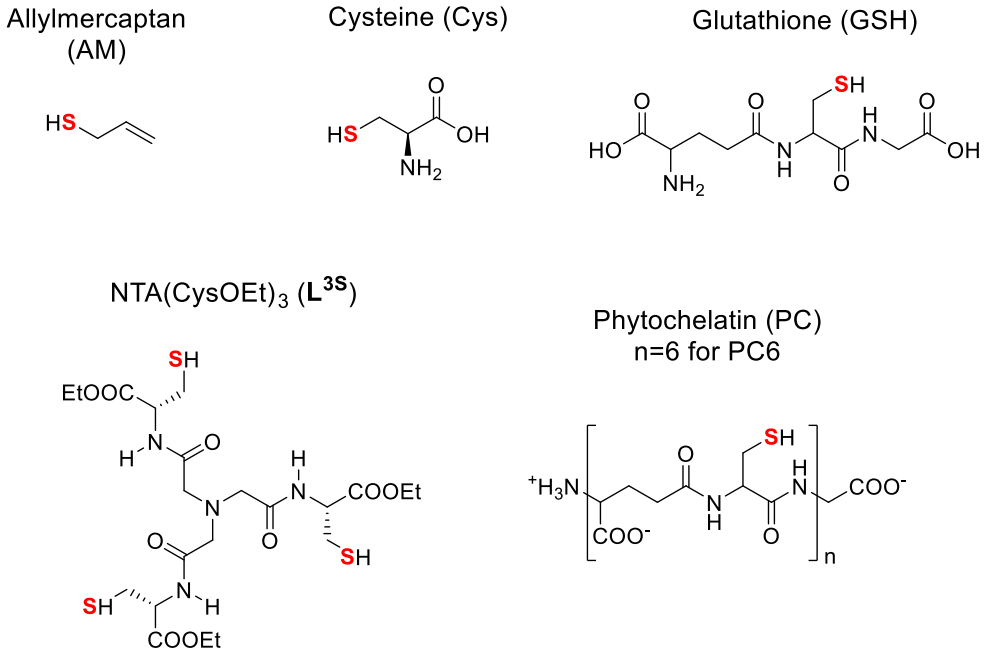

Glutathione (GSH) is a tripeptide bearing a cysteine (Cys) moiety, itself presenting a thiol R-SH function (Scheme 1). The spectrum of GSH in solution at pH 7.4 was measured in order to compare with the existing literature and to calibrate the energy scale (energy position of its absorption peak = 2473.7 eV). As shown in Figure 1A, the features of the spectrum of GSH are drastically modified when GSH reacts with Ag(I) in solution. An edge shift of -0.5 eV is observed as a consequence of the deprotonation of the thiol groups ($R\text{-}S^-$) and binding to Ag(I), along with a change in spectral features due to a change in the S coordination environment and geometry. According to previous Ag K-edge XAS and X-Ray Diffraction (XRD)

characterizations, the solution complex formed by Ag(I) and GSH is made of chains of repeated -Ag-S- units.[25,40] Therefore, the S atom in this complex shows a trigonal coordination with a C atom from the Cys moiety and two Ag(I) atoms, which we will refer to as R-S(-Ag)$_2$ in the following.

The observed energy shift and the spectral features of the Ag-GSH complex are consistent with the ones reported in the literature for other thiol- transition metal complexes.[41] Jalilehvand et al. showed that when Cys binds to metal ions with unfilled d orbitals (Cr(III), Ni(II), Mo(V)), S K-edge spectra show a pre-peak due to transitions to molecular orbitals with d character. In contrast, the spectra of complexes formed by Cys with Cd(II) and Hg(II), metals with filled d orbitals (d^{10}), show no pre-peak, a steep edge and a slower post-edge decrease. The spectral features of the Ag-GSH complex, where GS^- binds Ag(I) through its Cys moiety, are similar to those of Hg(II)-Cys and Cd(II)-Cys compounds, consistently with the fact that Ag(I) has no vacancies in the d-orbital (electron configuration [Kr] $4d^{10}$).

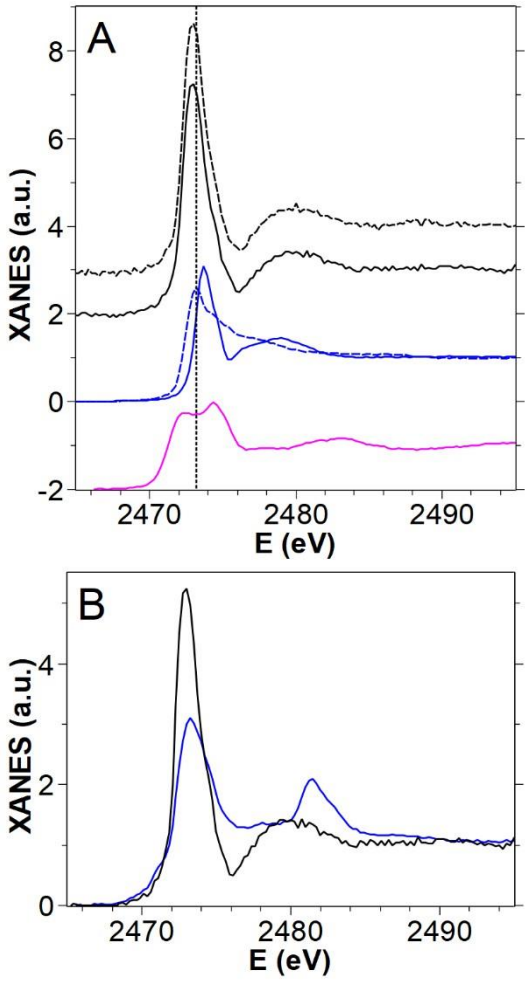

Figure 1. Sulfur K-edge XANES spectra of AgNPs assemblies and reference compounds. (A) AgNPs assemblies (black curves) of 40 nm (solid) and 200 nm (dashed); glutathione (blue curves) in solution at pH 7.4 alone (solid) and with Ag(I) (dashed); acanthite Ag_2S powder (magenta). The black dotted line indicates the energy of 2473.2 eV, corresponding to the peak position in the Ag-glutathione complex with R-S(-Ag)$_2$ ligation. (B) 40 nm assemblies measured as a frozen-hydrated (black) or dried (blue) drop.

The colloidal suspensions of AgNPs assemblies of 40 nm and 200 nm size provided the spectra reported in Fig. 1A as black solid and dashed lines, respectively. AgNPs assemblies are networks of 20 nm AgNPs bridged together by the bioinspired ligand $\mathbf{L^{3S}}$ represented in Scheme 1; we described the self-assembling reaction in a previous work, in which the resulting nanomaterial can be visualized thanks to cryogenic Transmission Electron Microscopy (cryo-TEM).[12] The XANES spectra of the two assemblies of different sizes overlap perfectly, meaning that the chemistry of S is independent of the size of the assembly, *i.e.* the surface phenomena occurring during self-assembling repeat themselves as the growth goes on. The peak position is 2472.9 eV, 0.3 eV lower than the peak position found in deprotonated R-S^- binding to Ag(I) ions (energy highlighted by a dotted vertical line in Fig. 1A). The most peculiar feature of the spectra of assemblies is their white line intensity: a transition of intensity > 5 in normalized spectra, never observed before, to the best of our knowledge. Previous works report the S K-edge XANES spectra of alkanethiol- or butanethiol-capped gold nanoparticles (AuNPs).[30,42,43] The XANES spectra presented in these works show two main peaks, separated by 7 eV, that the authors attributed to S-Au and S-C bonds, respectively. In contrast, the spectra of our AgNPs assemblies show a single low-energy transition that can be assigned to S-metal bonds, and no higher energy contributions. This discrepancy with the literature can be explained if we consider that our XAS experiment was performed on frozen-hydrated solutions, in contrast with previous experiments that were performed at room temperature on dried solutions. In order to investigate the effect of drying on the features of XAS spectra, we let a drop of 40 nm assemblies dry under N_2 atmosphere, and then we mounted it at room temperature on the XAS sample holder and measured it in the LN_2 cryostat to avoid beam-induced damage. The spectra of 40 nm assemblies measured as dried drops *vs* the ones measured on frozen-hydrated solutions are compared in Fig. 1B. Clearly, the drying has a dramatic effect on the S K-edge XAS spectrum: a low-energy peak at ~ 2473 eV, attributable to S-Ag bonds, is still present, but shows a much lower white-line intensity with respect to the hydrated sample, as a consequence of the lower proportion of surface-bound thiols in this specimen. The presence of self-absorption effects in the dried sample, as a consequence of the increase in concentration following water evaporation, cannot be excluded. Simultaneously, a high-energy transition at ~ 2481 eV, not present in hydrated samples, appears. The spectrum of the dried drop of 40 nm AgNPs assemblies shows the same features as the spectra of alkanethiols capped AuNPs.[30,42,43] Considering that the high-energy peak is present only in dried samples, we are inclined to think that it is not representative of S-C bonds (present in the thiolate moiety regardless of the sample hydration) as previously proposed, but rather of SO_x functions formed upon air-drying or beam damage. This hypothesis will be confirmed by SR-XPS experiments, where a spectral contribution assigned to SO_x species appear in air-dried samples, as reported in the SR-XPS section of this paper. In further support of our hypothesis, the energy of the white line position of sulfonate R-$S(=O)_2$-O^- species is 2481.3 eV.[44] The buffer we used, 2 mM citrate, contains no sulfur; however, the HEPES buffer of the initial $\mathbf{L^{3S}}$ stock solution presents a sulfonate group in its structure. Therefore, we cannot exclude that the contribution at ~ 2481 eV is due to residual HEPES, even though it seems unlikely considering the sample preparation protocol: as described in the Methods section, once the assemblies were formed we rinsed them three times by centrifugation in citrate buffer in order to remove HEPES as efficiently as possible. It must also be considered that we cautiously measured individual spectra on different spots of the drop of solution, and that sum spectra are obtained by merging spectra from different points.

Therefore, a cumulated beam damage can be ruled out. In addition, cryogenic measurements should limit radiation damage. Finally, we cannot exclude that some damage occurs in the span of an individual scan, although this hypothesis seems unlikely considering that the scan duration was only 32 s.

Interestingly, when organosulfur-coated AgNPs develop an intermediate crystalline silver sulfide (Ag_2S) layer, their S K-edge XAS spectrum does not show the preparation-dependent high energy feature reported in Fig. 1B, even if the colloidal suspension is dried and measured at room temperature.[15] This means that the Ag_2S layer that forms around the NPs passivates them and renders them less sensitive to the experimental protocol. In the case of AgNPs assemblies, the presence of an Ag_2S layer around the AgNP core is ruled out by the comparison between the spectra of assemblies and of bulk Ag_2S (black *vs* magenta spectra in Fig. 1A). This confirms the direct binding of the thiolate functions to surface Ag ions in AgNPs assemblies, as previously suggested by XPS measurements.[12] Our experimental evidence highlights that when the thiolate capping agent is directly bound to the NP surface, as it is in assemblies, it is crucial to measure the XAS spectra of frozen solutions in order to avoid preparation artifacts inducing sulfur oxidation into S=O species. This leads us to think that the spectral features of AgNPs assemblies presented here have never been observed before because this is the first example of metal-bound thiolates, with no intermediate layer, measured in non-altered conditions.

XANES deconvolution of complex AgNP-thiolate systems. The considerations reported above let us think that the S K-edge XANES spectrum of AgNPs assemblies is a model for thiolates bound to a silver surface ($R\text{-}S\text{-}Ag_{surf}$). As such, it can be used in the deconvolution of XAS spectra of complex mixtures of AgNPs and thiolate molecules, to measure the fraction of surface-bound $R\text{-}S^-$ functions. In order to verify this hypothesis, we acquired S K-edge XAS spectra of a panel of AgNPs-organosulfur mixtures and interpreted them thanks to Linear Combination Fitting (LCF) of reference compounds. As complex systems we chose (1) AgNPs-GSH solutions with Ag:S=1:1 stoichiometry and (2) allylmercaptan-coated silver nanoparticles (AgNPs@AM) synthesized starting with two different Ag:AM molar ratios. System (1) was prepared in anaerobic conditions, then frozen and measured in a LN_2–cooled cryostat. Such solutions in aerobic conditions are known to be unstable, as GSH promotes AgNPs oxidative dissolution.[24] In the absence of oxygen, we expect R-SH moieties to interact with surface Ag atoms without removing them from the nanoparticle, or to remain free in solution. In contrast, system (2) is a stable engineered nanomaterial, the structure of which has been deeply investigated.[16] It has been proposed that in AgNPs@AM systems the metallic Ag core of the nanoparticle is surrounded by a layer of crystalline Ag_2S and by AM grafted to this layer. As reference spectra we used the ones reported in Fig. 1A: GSH to represent free R-SH groups, Ag-GSH for S bridging two Ag atoms in a $R\text{-}S(\text{-}Ag)_2$ configuration, acanthite for the Ag_2S crystal structure, and AgNPs assemblies to represent thiolates directly grafted on the AgNP surface ($R\text{-}S\text{-}Ag_{surf}$). The experimental spectra of AgNPs-GSH solutions and of AgNPs@AM materials are reported in Figure 2 as dashed lines (black and blue, respectively).

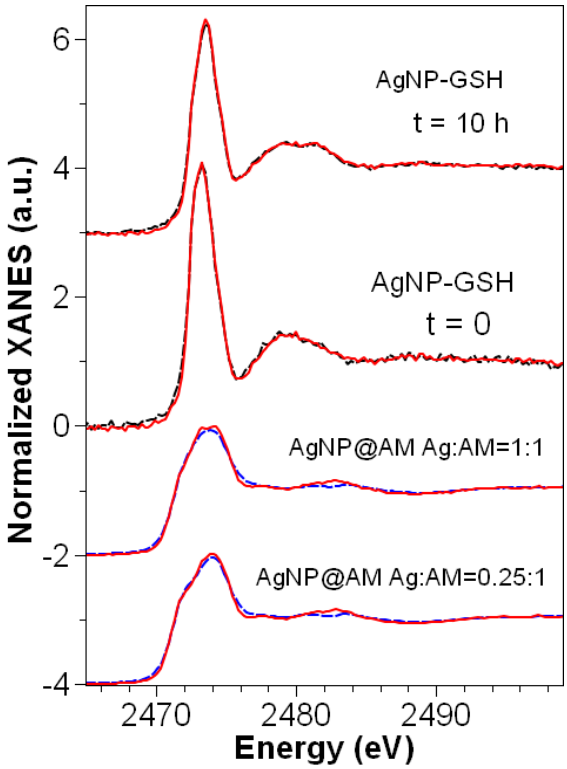

Figure 2. S K-edge XANES spectra of AgNPs-thiolate mixtures. Experimental (dashed lines) spectra of AgNP-GSH solutions (black) and allylmercaptan-coated AgNPs (blue). The relative best-fitting curves (solid red lines) based on linear combination fitting of reference compounds are reported on each experimental spectrum.

The AgNP-GSH mixture was measured immediately after preparation (t = 0) and after ten hours (t = 10 h) at room temperature in the glove box. We observe an evolution of the XANES spectrum over time (Fig. 2), consisting in the lowering and slight broadening of the main peak, which suggests an evolution of the system in anaerobic conditions. The LCF fitting results are reported in Table 1, and the relative best fitting curves in Fig. 2 (red curves over the corresponding experimental spectra): both AgNP-GSH solutions are the combination of two components, R-SH and R-S-Ag_{surf}, in different proportions depending on the incubation time. This means that an important fraction of GSH molecules (60%) deprotonate and bind to the AgNPs surface fast upon incubation, whereas the remaining fraction (40%) remains free in solution. In anaerobic conditions the system cannot evolve towards the oxidative dissolution of surface Ag(I), therefore it evolves towards the equilibrium between the two species R-SH and R-S-Ag_{surf}, reaching 63% of free thiols in solution upon 10 h. It must be noticed that in order to fit the high-energy region (~2482 eV) of the spectrum of the 10 h sample, a component corresponding to highly oxidized S had to be taken into account (R-S$(=O)_2$-O^- in table_LCF, spectrum available on the ID21 S XANES spectra database: https://www.esrf.eu/home/UsersAndScience/Experiments/XNP/ID21/php.html). This revealed the presence of a small percentage of oxidized S, equal to 3% of total S in the sample, most probably formed during sample transfer from the glove box to the cryostat. No Ag_2S component is detected in these samples, which allows us to exclude the occurrence of sulfidation reactions

as the ones observed in several environmental models.[18] The absence of the R-S(-Ag)$_2$ component, which would be the geometry of the Ag-GSH complex formed in solution, confirms that no Ag(I) release happens under anaerobic conditions.

Table 1. Results of the linear combination fitting analysis of S K-edge XANES spectra. The errors relative to the last digit are reported in parentheses.

	Ag_2S (%)	**R-SH** (%)	**R-S(-Ag)$_2$** (%)	**R-S-Ag$_{surf}$** (%)	**R-S(=O)$_2$-O$^-$** (%)	R_{fit} (10^{-3})
AgNP-GSH t=0	-	40 (1)	-	60 (1)	-	1.6
AgNP-GSH t=10h	-	63 (1)	-	34 (1)	3 (1)	0.5
AgNPs@AM (0.25:1)	77 (1)	-	23 (1)	-	-	1.3
AgNPs@AM (1:1)	73 (1)	-	27 (1)	-	-	1.4

AgNP@AM suspensions were measured at room temperature as previously described.[16] The experimental XANES spectra (Fig. 2, blue curves) of the two samples relative to Ag:AM molar ratios of 1:1 and 0.25:1 are similar to each other, and differ dramatically from the ones of AgNP-GSH solutions (black curves). However, no peak is observed at ~ 2481 eV, confirming that no preparation-dependent artifact is formed. LCF results confirm that the coordination of S is completely different in the two sets of AgNPs-thiolate systems: in the AgNPs@AM samples, S is found as Ag_2S and R-S(-Ag)$_2$, species that were not detected in the previous samples. These results are consistent with the previously proposed structure of AgNPs@AM materials based on XPS and Extended X-ray Absorption Fine Structure (EXAFS) analysis: the Ag(0) NP core is coated by an Ag_2S layer of variable thickness depending on the Ag/AM ratio, which is itself covered by AM molecules binding 2 Ag sites in a stapled configuration (here represented by the R-S(-Ag)$_2$ reference compound). The Ag-GSH compound measured here is confirmed as a model of R-S(-Ag)$_2$ geometry, regardless of the nature of the silver atoms: here Ag atoms are located at the surface of an Ag_2S crystalline structure, whereas in the Ag-GSH complex they are free Ag(I) in solution. The absence of an R-S-Ag$_{surf}$ component confirms that in AgNP@AM the thiol functions of AM do not bind directly to the AgNP surface.

This analysis shows that we dispose of a reliable and exhaustive set of compounds that allows one to unravel the fine details of the interaction between silver, ions or surfaces, and thiolate (bio-)molecules. We demonstrate that with a careful preparation and measurement protocol, and with an accurate set of reference compounds, it is possible to discern between sulfidized AgNPs and direct thiolate grafting to the surface. This has important implications in the characterization of engineered nanomaterials, for which a balance between surface functionalization and controlled Ag(I) release is required.

***Ab initio* simulations of XANES spectra.** The S K-edge absorption spectra of AgNPs assemblies (Fig. 1A) show peculiar and unprecedented features that deserve a more in-depth investigation. Experimental observations suggest that such features, consisting in a very sharp and narrow white line, originate from the electronic configuration of R-S$^-$ covalently bound to the silver surface atoms. In order to get more insight into the S-Ag surface interaction, we simulated *ab initio* the S K-edge XANES spectra of the Cys moiety (Scheme 1) grafted on a silver surface in different geometries. We chose the Ag(111) surface because thermodynamic

equilibrium shapes of monocrystalline AgNPs show a vast majority of this crystal planes in their surface with respect to Ag(100) and Ag(110) planes.[3] For the same reason, Density Functional Theory (DFT) studies that predict the adsorption geometry of thiolate on AgNPs and Ag surfaces, which provide valuable starting geometries for our *ab initio* XANES study, refer to the Ag(111) planes.[28,45]

According to the existing literature, thiolate molecules can graft to metal surfaces with three different binding modes called on-top, bridge, and hollow, meaning that each S can bind 1, 2 or 3 surface Ag atoms.[28,45,46] Considering this, three input clusters for cysteine grafted on an Ag(111) surface were built, as represented in Figure 3 from top and side view (A-B: on-top, C-D: bridge, E-F: hollow sites). The number of atoms in the cluster was such that all atoms fell within a sphere of 5.2 Å radius around the S absorber. This corresponded to three crystal planes. The simulation parameters were optimized over the spectra of reference compounds and fixed; relativistic calculations, including spin-orbit coupling, had to be adopted to reproduce the spectra relative to Cys-Ag(111) structures. The details are reported in the Supplementary Information.

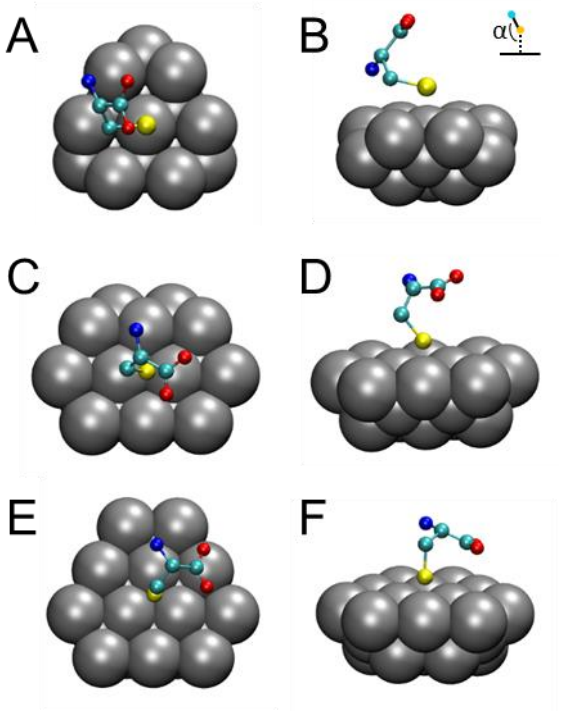

Figure 3. Graphical representation of Cys grafting on an Ag(111) surface. (A)-(B): on-top, (C)-(D): bridge, (E)-(F): hollow site. Left column: top view, Right column: side view.

Once the simulation parameters have been chosen, XANES spectra corresponding to several R-S-Ag(111) geometries were calculated, in order to help guess the most likely grafting geometry of $R\text{-}S^-$ to the NP surface in AgNPs assemblies and interpret the experimental observations.

Initial geometries were taken from a systematic DFT study of methanethiolate (CH_3S^-) adsorption on different AgNPs sites.[28] The Ag clusters considered in this theoretical study include from 13 atoms up to 309; in the largest cluster, the local environment experienced by

the adsorbate can be compared to an Ag(111) surface. This condition is necessary to mimic our systems, which are based on "large" AgNPs (20 nm diameter, corresponding to approximately 245000 atoms), where the adsorbate interacts with facets of the NP that can be approximated by silver surfaces.

Starting from the DFT-optimized geometries for the three possible binding modes, we investigated the influence of variations in Ag-S bond length and in the α angle on the calculated spectra, being α the angle between the S-C bond and the perpendicular to the surface (see Fig. 3). Selected spectra for the different geometries are reported in Figure 4, where the experimental spectrum of AgNPs assemblies is reported in panel A for comparison.

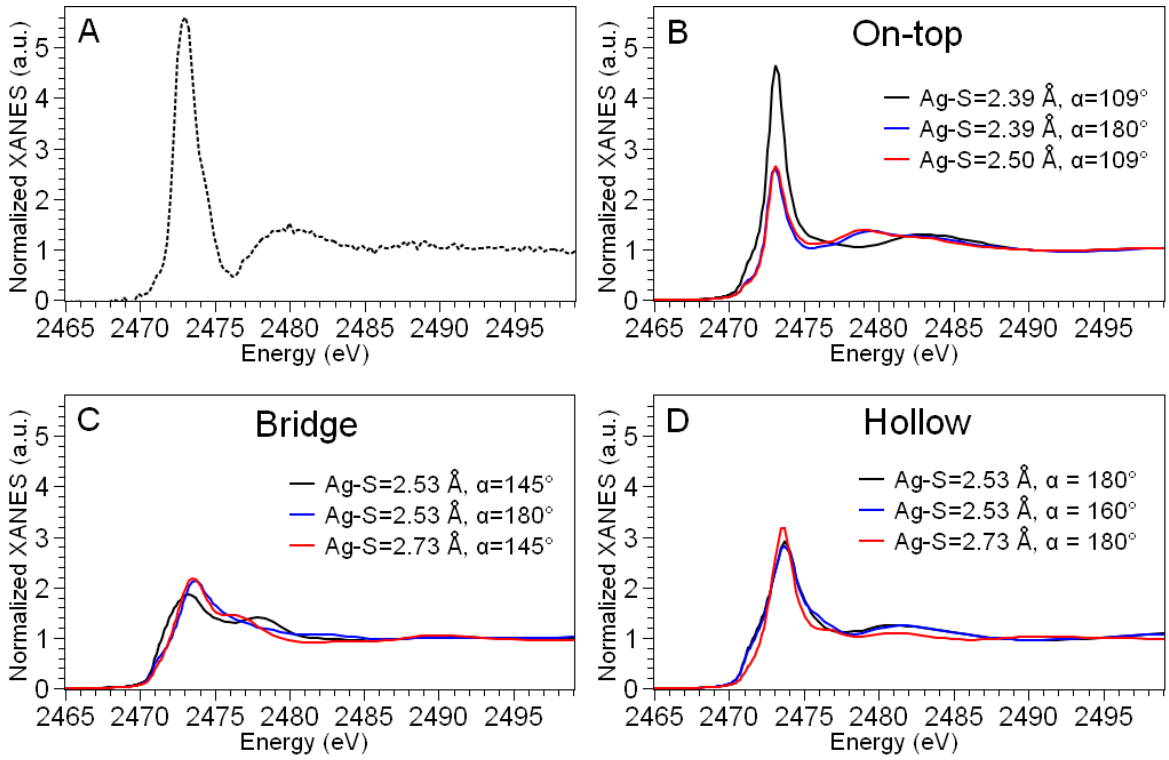

Figure 4. *Ab initio* simulation of S K-edge XANES spectra of a thiolate function grafted on Ag(111) surface. (A) Experimental spectrum of AgNPs assemblies. (B-D) Simulations of on-top (B), bridge (C), and hollow (D) grafting geometry with variable Ag-S distance and bending angle (α = angle between the S-C bond and the perpendicular to the Ag(111) surface). The axes ranges are the same in all graphs to compare the peaks' intensities and widths.

In Fig. 4B-D, the black curves represent the spectra generated starting from the Ag-S distance and α angle provided by Becerril et al. after DFT structural optimization, corresponding to the geometries visualized in Fig. 3.[28] Clearly, the geometry that best reproduces the experimental spectrum is the on-top geometry (panel B), which gives rise to a small pre-peak followed by a sharp and narrow white line, as in the experimental spectrum of AgNPs assemblies. The broad feature observed at 2480 eV is shifted to higher energy in the theoretical spectrum. However, being this feature due to multiple scattering contributions, its precise reproduction is extremely challenging and beyond the scope of this study. The normalized white line intensity for the on-

top site is slightly lower than the experimental one (~ 4.7 *vs* 5.6). Nevertheless, only this geometry can approach the surprisingly high value observed in the AgNPs assemblies sample. Starting from the on-top structure, we investigated the influence on the spectra of changes in the grafting geometry, moving the Cys molecule away from the surface (from 2.39 Å to 2.50 Å) or changing the tilt of the molecule with respect to the perpendicular to the surface (α from 109° to 180°). In Fig. 4B, we can see that these geometrical changes do not modify significantly the features of the XANES spectrum, but have a strong effect on its intensity. In other words, the shorter the Ag-S distance and the smaller the α angle (so the more tilted the Cys residue with respect to the direction perpendicular to the surface), the higher the white line intensity.

In the case of bridge sites (Fig. 4C), the initial geometry provides a low intensity white line (black curve, normalized white line intensity ~ 2) and a slow post-edge decrease. When the Cys residue is tilted in such a way that the S-C bond becomes perpendicular to the Ag(111) surface (α=180°), the general trend remains the same, while major modifications are observed in the post-edge spectral features (blue curve). However, none of the simulated bridge sites reproduces the experimental observations. Remarkably, the white line intensity and spectral features relative to R-S-Ag(111) models in bridge configuration are the same as the ones calculated for the molecular R-S-$(Ag)_2$ complex (Fig. S1) and experimentally measured in the Ag-GSH complex (Fig. 1A, blue dashed curve), where indeed the S atom bridges two Ag atoms. Hollow sites (Fig. 4D) produce a peaked white line, but without steep increase and broader than the experimental one. Moreover, the normalized white line intensity is of the order of 3, in contrast with experimental observations.

Based on the *ab initio* simulations results, the geometry that best reproduces the experimental data is an on-top binding site, where the S-C bond of Cys forms an angle of ~109° with the perpendicular to the surface. In this geometry, according to Sellers et al.,[46] the hybridization of the S atom is sp^3, and the bonding is more ionic in nature than in the more covalent hollow and bridge sites, and for this reason it is expected to be less stable. In hollow sites, in the case of methanethiolate (CH_3S^-) adsorption, the S-C bond is perpendicular to the Ag surface (α = 180°) and the S atoms show *sp* hybridization.[46] A more recent DFT study from Becerril et al. reported the adsorption energy of methanethiolate (CH_3S^-) on nanoparticles of different sizes represented as perfect icosahedra: bridge and hollow sites are energetically favored, whereas on-top sites are in general less likely. However, this study shows that on-top sites have relatively high adsorption probability in very small NPs (the Ag_{13} cluster) and on edge or vertexes between crystal planes.[28] This suggests that the on-top geometry could become more relevant the more the NP shows surface defects and the more it deviates from the approximation of perfect icosahedral shape. In addition, the DFT study concerns the very small molecule CH_3S^- and single molecule adsorption, neglecting the intermolecular interactions that play a crucial role in the determination of the thiolate binding mode.[47] Clearly, since XANES spectroscopy is sensitive to a cluster of ~5 Å around the absorber (sulfur in our case), such intermolecular long-range interactions cannot be predicted with our coupled experimental/theoretical approach. The tilt angle with respect to the surface, and therefore the hybridization of the S atom, depends on the thiol-bearing ligand, for instance on its size: the ligand architecture determines the interplay between long-range, molecule-molecule, and short-range, molecule-surface, Van der Waals interactions, as recently reviewed.[2] Another factor that is responsible for the hybridization of the grafted moieties is the reaction time between the substrate and the capping agent solution: in SAM of extremely low degree of coverage on Au surfaces, *sp* sites are favored for short and

sp^3 for long incubation times.[48] A similar phenomenon could lead to a majority of sp^3 sites in AgNPs assemblies, where the incubation time is relatively long (90 minutes before addition of a thiol blocking reagent to obtain 40 nm assemblies).

We previously reported of the hybridization of R-S-Ag_{surf} species in purified AgNPs assemblies: SR-XPS measurements demonstrated that 60% or more of $R\text{-}S^-$ groups in assemblies are bonded to the AgNPs surface, equally distributed between *sp* and sp^3 hybridization sites.[12] This highlights that on-top sites, although less stable than hollow and bridge sites, are an important component in the interaction between $R\text{-}S^-$ functions and AgNPs surfaces. The comparison between experimental and theoretical S K-edge XANES spectra suggest that on-top sites with sp^3 hybridization are predominant, but clearly the presence of other adsorption sites in lower proportion is expected. It must also be considered that some discrepancies can arise between XPS and XAS results for two main reasons, one of which is that SR-XPS probes the first ~1 nm of the material, whereas XAS has a higher penetration depth that probes the whole specimen. For instance, considering that assemblies are 3D objects made of 20 nm AgNPs bridged together by the **L^{3S}** ligand, if on-top adsorption sites were buried in the interior of the assembly while sp-like sites were more external, this would results in an overestimation of the fraction of sp hybridized sites. The second reason is that, due to the experimental requirements of each technique, the sample preparation and measurement conditions were not the same: XPS data were acquired on dried drops, which can partially modify the chemistry of surface-bound thiols, as we previously demonstrated. Overall, the *ab initio* simulation of XANES spectra suggest that sp^3 hybridized adsorption sites are an important component of the thiol-metal interface in AgNPs assemblies.

Synchrotron Radiation X-ray Photoelectron Spectroscopy (SR-XPS). XPS can dissect the fine details of the metal-sulfur interface in thiol-capped AgNPs. Therefore we made use of this technique to probe the early stage of thiolate adsorption on AgNPs in the presence of the **L^{3S}** molecule, system that evolves towards self-assembling. As the first instance, C 1s spectra were analyzed in order to disclose the interaction of **L^{3S}** with citrate-stabilized NPs suspension. We analyzed C 1s core-level spectra of citrate-stabilized AgNPs alone or in the presence of the **L^{3S}** ligand. The spectra of the buffer solution, of AgNPs, and of the AgNPs-**L^{3S}** solution (Figure 5) show four common components centered at different Binding Energies (BE), due to aliphatic C-C (blue, BE = 285.0 eV), C-O from adventitious carbon (cyan, BE = 285.8 eV), COH/CH_2 (magenta, BE = 286.8 eV), COO^-Na^+ (black, E=288.3 eV), compatible with the buffer composition (2 mM Na-citrate) and with the presence of adventitious carbon. A low intensity component at 289.9 eV, assigned to free R-COO(H), is present only in the AgNPs sample (orange curve).[49] The absence of a shake-up satellite at 297 eV (not shown) in the AgNPs samples confirms the absence of tannic acid, used as a stabilizer during synthesis, in the final colloidal suspension. In the AgNPs sample we observe the appearance of a contribution at 287.8 eV, not present in the buffer, assigned to coordinated carboxylates (COO-Ag, green curve), as previously observed in case of citrate-stabilized AuNPs.[49] In the AgNPs-**L^{3S}** solution, the component due to coordinated carboxylates is not observed, most probably because of the replacement of $R\text{-}COO^-$ with $R\text{-}S^-$ moieties at the NP surface. This replacement has already been observed in Cit-AuNPs capped with Cys, and sheds light on the mechanism of formation of the capping layer.[50]

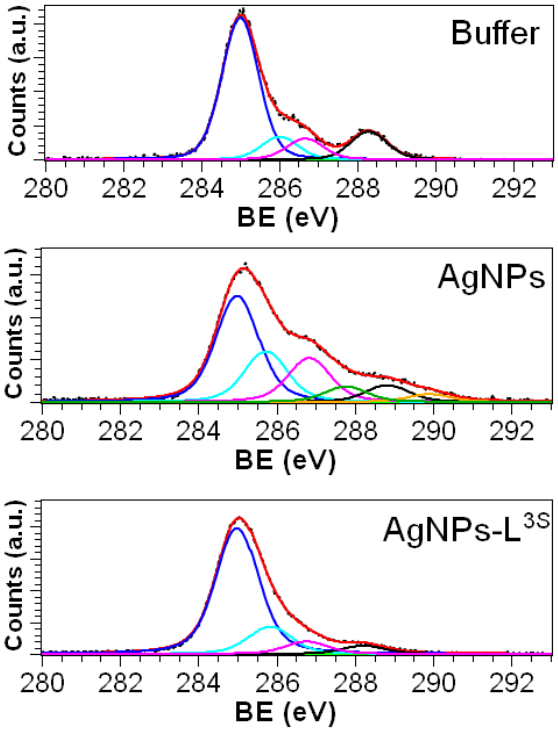

Figure 5. SR-XPS spectra of C 1s core level for the 2 mM Na-citrate buffer solution, uncoated AgNPs, and the **L**^{3S}-AgNPs solution. Best-fitting curves are reported in red over the corresponding experimental spectrum (black dots). Individual Voigt components contributing to the final fit are reported on each graph (blue, cyan, magenta, green, black, orange solid curves). Photon energy 596 eV.

Upon binding to the AgNP surface, the ligand **L**^{3S} promotes a self-assembling process that leads to the formation of stable AgNPs assemblies; in contrast, other thiol-bearing molecules as GSH or phytochelatines (PC), polymers of glutathione units, induce the dissolution of the AgNPs and the release of Ag(I) in solution.[24] We hypothesize that the grafting mode of the thiolate function to the AgNPs surface, itself driven by the size and solution properties of the thiol molecule,[2] could be responsible for the stabilization *vs* dissolution behavior. Therefore, we investigated the early stages of surface grafting in the AgNPs-**L**^{3S} solution and in the AgNPs-phytochelatine-6 (PC6) solution. The latter is a polymer made of 6 GSH units (see Scheme 1), which induces dissolution of AgNPs at a much faster rate than GSH alone.[24] We chose PC6 in order to maximize the dissolution effect and have the highest variability with respect to the AgNPs-**L**^{3S} solution. The NPs-ligands complexes were formed in solution at room temperature, in a glove-bag in order to minimize sulfur oxidation, then deposited on Au-coated Si wafers in air at room temperature and allowed to dry for 30 minutes before analysis. For comparison, also the molecular complex Ag**L**^{3S}, where Ag(I) binds to three thiolates in trigonal coordination,[22] was characterized. The S 2p core-level spectra are reported in Figure 6 and show that four contributions were identified in all samples. The most intense in the NPs-ligands solutions has the maximum of the S $2p_{3/2}$ component centered at 163.4 eV (solid black curves), which is assigned to unbound thiols (R-SH).[51] These are the groups from the ligands that have not attached to the surface yet, since the reactions are in their early stages. A second component is found around 164.1 eV in all samples (cyan) and assigned to disulfide bonds (RS-SR). This

component represents a minor fraction of all S species in NPs-ligand systems (< 12%, Table 2). A contribution from S=O containing species appears at ~ 168 eV (magenta). The observation of this component confirms what we observed in S K-edge XANES, where we detected sulfonates in dried drops. Interestingly, all spectra exhibit this spectral contribution, regardless of the presence of $\mathbf{L}^{3S}$ in the sample. Considering that only $\mathbf{L}^{3S}$ could be responsible for sulfonate contamination (since it was initially dissolved in sulfonate-containing HEPES buffer, as discussed in the previous sections), we can conclude that the sulfonates are not due to a contamination, but they are either formed during drying or under the photon beam.

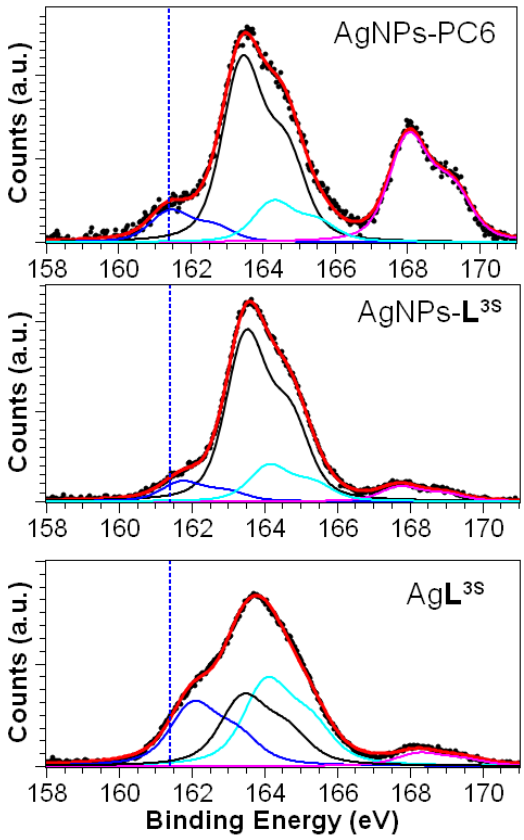

Figure 6. SR-XPS S 2p core levels spectra acquired using 380 eV photon energy. The samples are AgNPs in solution with phytochelatin-6 (PC6) or the $\mathbf{L}^{3S}$ ligand, and the complex formed by $\mathbf{L}^{3S}$ with ionic silver (Ag$\mathbf{L}^{3S}$). Best-fitting curves are reported in red over the corresponding experimental spectrum (black dots). Individual Voigt doublets contributing to the final fit are reported on each graph (blue, black, cyan, and magenta solid lines). The blue dashed vertical lines indicate the BE of 161.44 eV in all graphs.

The most interesting signal for our purposes is the one with the maximum of the S $2p_{3/2}$ component between 161 eV and 162 eV (blue), assigned to R-S-Ag species, *i.e.* thiolate functions grafted to the NP surface. The BE relative to this spin-orbit doublet spans over 0.6 eV between the three complexes. The value of 162.0 eV, observed in the molecular Ag$\mathbf{L}^{3S}$ complex, can be assigned to R-S^- groups covalently bound to Ag or Au in sp^3 hybridization.[6,46,48] In the NPs-ligand samples, the component assigned to thiolates grafted to the NP surface (R-S-Ag) represents less than 10% of total S species (Table 2). Therefore, it is

not possible to decompose it into two distinct signals due to *sp* and sp^3 hybridization, as reported in previous studies.[6,12] It must be considered that the SR-XPS spectra that we reported in a recent work, show a higher proportion of surface-grafted thiolates because they refer to purified AgNPs assemblies, *i.e.* highly homogeneous samples in which the self-assembling reaction of AgNPs triggered by $\mathbf{L^{3S}}$ is completed.[12] Here, in contrast, we investigate the early stages of the reaction between AgNPs and $\mathbf{L^{3S}}$, which explains why only a small fraction of the thiolates are bound to the surface. According to the above-mentioned studies, thiolates grafted to Au or Ag surfaces with *sp* orbital hybridization (i.e. forming a surface-S-C angle of ~ 180°) give rise to a lower BE signal than sp^3-hybridized S. The associated BE value ranges between 161.1 eV and 161.4 eV in previous studies.[6] More in general, independently on the energy calibration, the BE difference between the signals relative to pure *sp* and pure sp^3 hybridization is expected to be ~1 eV.[48] The BE values measured in the NP-ligands solutions reveal a shift in the spin-orbit doublet (see position of the blue curves with respect to the blue dashed line in Fig. 6), and suggest a slightly different proportion of sp/sp^3 binding sites in different AgNPs-thiolate systems in the early stages of the reaction at the NP surface. However, this BE difference is of only 0.33 eV (BE= 161.44 eV in AgNP-PC6 *vs* BE= 161.77 eV in AgNP-$\mathbf{L^{3S}}$), which allows us to exclude a completely different adsorption geometry for the two ligands promoting assembling and dissolution, respectively.

Table 2. Band assignment and semi-quantitative analysis of XPS S 2p core level spectra.

SAMPLE	$S2p_{3/2}$ BE (eV)	Atomic %	FWHM (eV)	Assignment
AgNP-PC6	161.44	8.73	1.1	R-S-Ag
	163.43	50.32	1.1	R-SH
	164.29	11.30	1.1	RS-SR
	168.04	29.64	1.1	SO_x
AgNP-$\mathbf{L^{3S}}$	161.77	8.34	1.3	R-S-Ag
	163.49	70.25	1.3	R-SH
	164.12	15.20	1.3	RS-SR
	168.06	6.21	1.3	SO_x
Ag$\mathbf{L^{3S}}$	162.02	27.10	1.5	R-S-Ag
	163.41	30.18	1.5	R-SH
	164.06	37.03	1.5	RS-SR
	168.24	5.69	1.5	SO_x

It has been reported that in SAM of alkanethiols ($CH_3{-}C_6H_4{-}C_6H_4{-}(CH_2)_m{-}SH$, m = 1−6) on Ag and Au polycrystalline surfaces, the chain length determines the sulfur atom hybridization, which in turn influences the surface coverage.[52] Also in the case of thiolate SAMs on Au(111) monolayers, the chain length plays a role in the ligand packing and surface coverage, since it affects the ligand intermolecular interactions.[47] The interplay between intermolecular interactions and the preferential geometry of the S-metal bond determines the final hybridization of the S atom. Thus, it is reasonable to expect different proportions of sp/sp^3 hybridized S atoms grafted to the AgNPs surfaces when different thiol-bearing ligands are observed, as suggested by SR-XPS. Indeed, the very different ligand conformations (PC6 being a linear chain whereas $\mathbf{L^{3S}}$ is a tripodal molecule, see Scheme 1) can give rise to different intermolecular interactions that drive the ligand arrangement at the surface. Nevertheless, it is

surprising to observe that the difference in *sp/sp*^{3} sites is very small, at the limit of the resolution, in spite of the opposite behavior observed in the two systems: NP dissolution in presence of PC6, self-assembly with $\mathbf{L^{3S}}$. These data suggest that the metal-thiol binding mode is not the only factor that determines the stability of the AgNP-thiolate ligand system, and other hypothesis need to be investigated, for instance concerning the ligand architecture and its solution properties.

CONCLUSIONS

Our work sheds light into the metal-ligand interface by finely dissecting the details of Ag-S bonds. We demonstrated the efficiency of the method on two distinct complex systems including a stable engineered nanomaterial and an unstable AgNP-thiolate solution that releases Ag(I) ions over time. We highlighted the importance of cryogenic analysis in order to probe the unaltered metal-thiol interface. Thanks to S K-edge XANES in cryogenic conditions, we provide a model system in which thiolates are grafted directly on the nanoparticle surface, which is unambiguously distinguished from other systems presenting an intermediate silver sulfide layer. This might have applications in nanotechnology by enabling the precise characterization of complex systems such as core@shell NPs. Moreover, it helps the design of future thiol-capped AgNPs with desired properties, with a fine control of ion release driven already from the synthesis steps.

SUPPORTING INFORMATION

Details of the *ab initio* calculations are available free of charge as Supporting Information on the ACS Publications website.

AUTHOR INFORMATION

Corresponding author

*E-mail: giulia.veronesi@cea.fr Phone number: +33 438 78 48 48.

ACKNOWLEDGEMENT

The authors thank Hiram Castillo-Michel, Murielle Salomé, Marine Cotte for sharing in-house beamtime and for their help on the ID21 beamline of the ESRF; Carlo Meneghini for the S K-edge XANES spectra of AgNPs@AM; Ana Elena Pradas del Real for the acanthite Ag_2S powder. The research leading to these results has received funding from the University Grenoble Alpes through the NanoBIS project (call IDEX: IRS - CBS-2017) and from the European Community's Seventh Framework Programme (FP7/2007-2013) under grant agreement nº 312284. This work is supported by the LabEx SERENADE (grant ANR-11-LABX-0064) and the LabEx ARCANE and CBH-EUR-GS (grant ANR-17-EURE-0003). SN and IP gratefully acknowledge financial support from EUROFEL funds and the technical support of Federico Salvador and Paolo Bertoch.

REFERENCES

(1) Love, J. C.; Estroff, L. A.; Kriebel, J. K.; Nuzzo, R. G.; Whitesides, G. M. Self-Assembled Monolayers of Thiolates on Metals as a Form of Nanotechnology. *Chem. Rev.* **2005**, *105*, 1103–1170.

(2) Vericat, C.; Vela, M. E.; Corthey, G.; Pensa, E.; Cortés, E.; Fonticelli, M. H.; Ibañez, F.; Benitez, G. E.; Carro, P.; Salvarezza, R. C. Self-Assembled Monolayers of Thiolates on Metals: A Review Article on Sulfur-Metal Chemistry and Surface Structures. *RSC Adv* **2014**, *4*, 27730–27754.

(3) Azcárate, J. C.; Corthey, G.; Pensa, E.; Vericat, C.; Fonticelli, M. H.; Salvarezza, R. C.; Carro, P. Understanding the Surface Chemistry of Thiolate-Protected Metallic Nanoparticles. *J. Phys. Chem. Lett.* **2013**, *4*, 3127–3138.

(4) Malinsky, M. D.; Kelly, K. L.; Schatz, G. C.; Van Duyne, R. P. Chain Length Dependence and Sensing Capabilities of the Localized Surface Plasmon Resonance of Silver Nanoparticles Chemically Modified with Alkanethiol Self-Assembled Monolayers. *J. Am. Chem. Soc.* **2001**, *123*, 1471–1482.

(5) Stewart, A.; Zheng, S.; McCourt, M. R.; Bell, S. E. J. Controlling Assembly of Mixed Thiol Monolayers on Silver Nanoparticles to Tune Their Surface Properties. *ACS Nano* **2012**, *6*, 3718–3726.

(6) Venditti, I.; Testa, G.; Sciubba, F.; Carlini, L.; Porcaro, F.; Meneghini, C.; Mobilio, S.; Battocchio, C.; Fratoddi, I. Hydrophilic Metal Nanoparticles Functionalized by 2-Diethylaminoethanethiol: A Close Look at the Metal–Ligand Interaction and Interface Chemical Structure. *J. Phys. Chem. C* **2017**, *121*, 8002–8013.

(7) Prosposito, P.; Burratti, L.; Bellingeri, A.; Protano, G.; Faleri, C.; Corsi, I.; Battocchio, C.; Iucci G.; Tortora L.; Secchi, V.; et al. Bifunctionalized Silver Nanoparticles as Hg^{2+} Plasmonic Sensor in Water: Synthesis, Characterizations, and Ecosafety. *Nanomaterials* **2019**, *9*, 1353.

(8) Le Ouay, B.; Stellacci, F. Antibacterial Activity of Silver Nanoparticles: A Surface Science Insight. *Nano Today* **2015**, *10*, 339–354.

(9) Sotiriou, G. A.; Pratsinis, S. E. Antibacterial Activity of Nanosilver Ions and Particles. *Environ. Sci. Technol.* **2010**, *44*, 5649–5654.

(10) Marchioni, M.; Jouneau, P.-H.; Chevallet, M.; Michaud-Soret, I.; Deniaud, A. Silver Nanoparticle Fate in Mammals: Bridging in Vitro and in Vivo Studies. *Coord. Chem. Rev.* **2018**, *364*, 118–136.

(11) Liu, J.; Sonshine, D. A.; Shervani, S.; Hurt, R. H. Controlled Release of Biologically Active Silver from Nanosilver Surfaces. *ACS Nano* **2010**, *4*, 6903–6913.

(12) Marchioni, M.; Veronesi, G.; Worms, I.; Ling, W. L.; Gallon, T.; Leonard, D.; Gateau, C.; Chevallet, M.; Jouneau, P.-H.; Carlini, L.; et al. Safer-by-Design Biocides Made of Tri-Thiol Bridged Silver Nanoparticle Assemblies. *Nanoscale Horiz.* **2020**, *5*, 507–513.

(13) Amato, E.; Diaz-Fernandez, Y. A.; Taglietti, A.; Pallavicini, P.; Pasotti, L.; Cucca, L.; Milanese, C.; Grisoli, P.; Dacarro, C.; Fernandez-Hechavarria, J. M.; et al. Synthesis, Characterization and Antibacterial Activity against Gram Positive and Gram Negative Bacteria of Biomimetically Coated Silver Nanoparticles. *Langmuir* **2011**, *27*, 9165–9173.

(14) Girón, J. V. M.; Zelaya, E.; Rubert, A.; Benítez, G.; Carro, P.; Salvarezza, R. C.; Vela, M. E. Surface Chemistry of 4-Mercaptobenzoic Acid Self-Assembled on Ag(111) and Ag Nanoparticles. *J. Phys. Chem. C* **2013**, *117*, 24967–24974.

(15) Padmos, J. D.; Zhang, P. Surface Structure of Organosulfur Stabilized Silver Nanoparticles Studied with X-Ray Absorption Spectroscopy. *J. Phys. Chem. C* **2012**, *116*, 23094–23101.

(16) Battocchio, C.; Meneghini, C.; Fratoddi, I.; Venditti, I.; Russo, M. V.; Aquilanti, G.; Maurizio, C.; Bondino, F.; Matassa, R.; Rossi, et al. Silver Nanoparticles Stabilized with Thiols: A Close Look at the Local Chemistry and Chemical Structure. *J. Phys. Chem. C* **2012**, *116*, 19571–19578.

(17) Munaro, J.; Dolcet, P.; Nappini, S.; Magnano, E.; Dengo, N.; Lucchini, G.; Speghini, A.; Gross, S. The Role of the Synthetic Pathways on Properties of Ag_2S Nanoparticles for Photothermal Applications. *Appl. Surf. Sci.* **2020**, *514*, 145856.

(18) Levard, C.; Hotze, E. M.; Lowry, G. V.; Brown, G. E. Environmental Transformations of Silver Nanoparticles: Impact on Stability and Toxicity. *Environ. Sci. Technol.* **2012**, *46*, 6900–6914.

(19) Pradas del Real, A. E.; Castillo-Michel, H.; Kaegi, R.; Sinnet, B.; Magnin, V.; Findling, N.; Villanova, J.; Carrière, M.; Santaella, C.; Fernández-Martínez, A.; et al. Fate of Ag-NPs in Sewage Sludge after Application on Agricultural Soils. *Environ. Sci. Technol.* **2016**, *50*, 1759–1768.

(20) Porcaro, F.; Carlini, L.; Ugolini, A.; Visaggio, D.; Visca, P.; Fratoddi, I.; Venditti, I.; Meneghini, C.; Simonelli, L.; Marini, C.; et al. Synthesis and Structural Characterization of Silver Nanoparticles Stabilized with 3-Mercapto-1-Propansulfonate and 1-Thioglucose Mixed Thiols for Antibacterial Applications. *Materials* **2016**, *9*, 1028.

(21) Pujol, A. M.; Gateau, C.; Lebrun, C.; Delangle, P. A Cysteine-Based Tripodal Chelator with a High Affinity and Selectivity for Copper(I). *J. Am. Chem. Soc.* **2009**, *131*, 6928–6929.

(22) Veronesi, G.; Gallon, T.; Deniaud, A.; Boff, B.; Gateau, C.; Lebrun, C.; Vidaud, C.; Rollin-Genetet, F.; Carrière, M.; Kieffer, I.; et al. XAS Investigation of Silver(I) Coordination in Copper(I) Biological Binding Sites. *Inorg. Chem.* **2015**, *54*, 11688–11696.

(23) Gondikas, A. P.; Morris, A.; Reinsch, B. C.; Marinakos, S. M.; Lowry, G. V.; Hsu-Kim, H. Cysteine-Induced Modifications of Zero-Valent Silver Nanomaterials: Implications for Particle Surface Chemistry, Aggregation, Dissolution, and Silver Speciation. *Environ. Sci. Technol.* **2012**, *46*, 7037–7045.

(24) Marchioni, M.; Gallon, T.; Worms, I.; Jouneau, P.-H.; Lebrun, C.; Veronesi, G.; Truffier-Boutry, D.; Mintz, E.; Delangle, P.; Deniaud, A.; et al. Insights into Polythiol-Assisted AgNP Dissolution Induced by Bio-Relevant Molecules. *Env. Sci Nano* **2018**, *5*, 1911–1920.

(25) Veronesi, G.; Aude-Garcia, C.; Kieffer, I.; Gallon, T.; Delangle, P.; Herlin-Boime, N.; Rabilloud, T.; Carrière, M. Exposure-Dependent Ag^+ Release from Silver Nanoparticles and Its Complexation in AgS_2 Sites in Primary Murine Macrophages. *Nanoscale* **2015**, *7*, 7323–7330.

(26) Veronesi, G.; Deniaud, A.; Gallon, T.; Jouneau, P.-H.; Villanova, J.; Delangle, P.; Carrière, M.; Kieffer, I.; Charbonnier, P.; Mintz, E.; et al. Visualization, Quantification and Coordination of Ag^+ Ions Released from Silver Nanoparticles in Hepatocytes. *Nanoscale* **2016**, *8*, 17012–17021.

(27) Tardillo Suárez, V.; Karepina, E.; Chevallet, M.; Gallet, B.; Cottet-Rousselle, C.; Charbonnier, P.; Moriscot, C.; Michaud-Soret, I.; Bal, W.; Fuchs, A.; et al. Nuclear Translocation of Silver Ions and Hepatocyte Nuclear Receptor Impairment upon Exposure to Silver Nanoparticles. *Environ. Sci. Nano* **2020**, *7*, 1373–1387.

(28) Becerril, D.; Noguez, C. Adsorption of a Methylthio Radical on Silver Nanoparticles: Size Dependence. *J. Phys. Chem. C* **2015**, *119*, 10824–10835.

(29) Kano, S.; Tada, T.; Majima, Y. Nanoparticle Characterization Based on STM and STS. *Chem. Soc. Rev.* **2015**, *44*, 970–987.

(30) Ramallo-López, J. M.; Giovanetti, L. J.; Vicentin, F. C.; Requejo, F. G. XANES Study of the Radiation Damage on Alkanethiolates-Capped Au Nanoparticles. *J. Phys. Conf. Ser.* **2013**, *430*, 012034.

(31) Bastús, N. G.; Merkoçi, F.; Piella, J.; Puntes, V. Synthesis of Highly Monodisperse Citrate-Stabilized Silver Nanoparticles of up to 200 Nm: Kinetic Control and Catalytic Properties. *Chem. Mater.* **2014**, *26*, 2836–2846.

(32) Cotte, M.; Pouyet, E.; Salomé, M.; Rivard, C.; De Nolf, W.; Castillo-Michel, H.; Fabris, T.; Monico, L.; Janssens, K.; Wang, T.; et al. The ID21 X-Ray and Infrared Microscopy Beamline at the ESRF: Status and Recent Applications to Artistic Materials. *J Anal Spectrom* **2017**, *32*, 477–493.

(33) Ravel, B.; Newville, M. ATHENA, ARTEMIS, HEPHAESTUS: Data Analysis for X-Ray Absorption Spectroscopy Using IFEFFIT. *J Synchrotron Radiat* **2005**, *12*, 537–541.

(34) Bunău, O.; Joly, Y. Self-Consistent Aspects of x-Ray Absorption Calculations. *J. Phys. Condens. Matter* **2009**, *21*, 345501.

(35) Guda, S. A.; Guda, A. A.; Soldatov, M. A.; Lomachenko, K. A.; Bugaev, A. L.; Lamberti, C.; Gawelda, W.; Bressler, C.; Smolentsev, G.; Soldatov, A. V.; et al. Optimized Finite Difference Method for the Full-Potential XANES Simulations: Application to Molecular Adsorption Geometries in MOFs and Metal–Ligand Intersystem Crossing Transients. *J. Chem. Theory Comput.* **2015**, *11*, 4512–4521.

(36) Amestoy, P. R.; Guermouche, A.; L'Excellent, J.-Y.; Pralet, S. Hybrid Scheduling for the Parallel Solution of Linear Systems. *Parallel Comput.* **2006**, *32*, 136–156.

(37) Allen, F. H. The Cambridge Structural Database: A Quarter of a Million Crystal Structures and Rising. *Acta Crystallogr. Sect. B* **2002**, *58*, 380–388.
(38) Zangrando, M.; Zacchigna, M.; Finazzi, M.; Cocco, D.; Rochow, R.; Parmigiani, F. Polarized High-Brilliance and High-Resolution Soft x-Ray Source at ELETTRA: The Performance of Beamline BACH. *Rev. Sci. Instrum.* **2004**, *75*, 31–36.
(39) Libra, J. *KolXPD, Software for Spectroscopy Data Measurement and Processing*, version 1.8.0. (build 61), https://www.kolibrik.net/kolxpd/.
(40) Leung, B. O.; Jalilehvand, F.; Mah, V.; Parvez, M.; Wu, Q. Silver(I) Complex Formation with Cysteine, Penicillamine, and Glutathione. *Inorg. Chem.* **2013**, *52*, 4593–4602.
(41) Jalilehvand, F. Sulfur: Not a "Silent" Element Any More. *Chem Soc Rev* **2006**, *35*, 1256–1268.
(42) Ramallo-López, J. M.; Giovanetti, L. J.; Requejo, F. G.; Isaacs, S. R.; Shon, Y. S.; Salmeron, M. Molecular Conformation Changes in Alkylthiol Ligands as a Function of Size in Gold Nanoparticles: X-Ray Absorption Studies. *Phys. Rev. B* **2006**, *74*, 073410.
(43) Grumelli, D.; Vericat, C.; Benitez, G.; Vela, M. E.; Salvarezza, R. C.; Giovanetti, L. J.; Ramallo-López, J. M.; Requejo, F. G.; Craievich, A. F.; Shon, Y. S. Thiol-Capped Gold Nanoparticles on Graphite: Spontaneous Adsorption and Electrochemically Induced Release. *J. Phys. Chem. C* **2007**, *111*, 7179–7184.
(44) Prietzel, J.; Botzaki, A.; Tyufekchieva, N.; Brettholle, M.; Thieme, J.; Klysubun, W. Sulfur Speciation in Soil by S K-Edge XANES Spectroscopy: Comparison of Spectral Deconvolution and Linear Combination Fitting. *Environ. Sci. Technol.* **2011**, *45*, 2878–2886.
(45) Cometto, F. P.; Paredes-Olivera, P.; Macagno, V. A.; Patrito, E. M. Density Functional Theory Study of the Adsorption of Alkanethiols on Cu(111), Ag(111), and Au(111) in the Low and High Coverage Regimes. *J. Phys. Chem. B* **2005**, *109*, 21737–21748.
(46) Sellers, H.; Ulman, A.; Shnidman, Y.; Eilers, J. E. Structure and Binding of Alkanethiolates on Gold and Silver Surfaces: Implications for Self-Assembled Monolayers. *J. Am. Chem. Soc.* **1993**, *115*, 9389–9401.
(47) Tao, Y.-T.; Wu, C.-C.; Eu, J.-Y.; Lin, W.-L.; Wu, K.-C.; Chen, C. Structure Evolution of Aromatic-Derivatized Thiol Monolayers on Evaporated Gold. *Langmuir* **1997**, *13*, 4018–4023.
(48) Ishida, T.; Hara, M.; Kojima, I.; Tsuneda, S.; Nishida, N.; Sasabe, H.; Knoll, W. High Resolution X-Ray Photoelectron Spectroscopy Measurements of Octadecanethiol Self-Assembled Monolayers on Au(111). *Langmuir* **1998**, *14*, 2092–2096.
(49) Park, J.-W.; Shumaker-Parry, J. S. Structural Study of Citrate Layers on Gold Nanoparticles: Role of Intermolecular Interactions in Stabilizing Nanoparticles. *J. Am. Chem. Soc.* **2014**, *136*, 1907–1921.
(50) Majzik, A.; Fülöp, L.; Csapó, E.; Bogár, F.; Martinek, T.; Penke, B.; Bíró, G.; Dékány, I. Functionalization of Gold Nanoparticles with Amino Acid, β-Amyloid Peptides and Fragment. *Colloids Surf. B Biointerfaces* **2010**, *81*, 235–241.
(51) Castner, D. G.; Hinds, K.; Grainger, D. W. X-Ray Photoelectron Spectroscopy Sulfur 2p Study of Organic Thiol and Disulfide Binding Interactions with Gold Surfaces. *Langmuir* **1996**, *12*, 5083–5086.
(52) Rong, H.-T.; Frey, S.; Yang, Y.-J.; Zharnikov, M.; Buck, M.; Wühn, M.; Wöll, C.; Helmchen, G. On the Importance of the Headgroup Substrate Bond in Thiol Monolayers: A Study of Biphenyl-Based Thiols on Gold and Silver. *Langmuir* **2001**, *17*, 1582–1593.

ToC Image

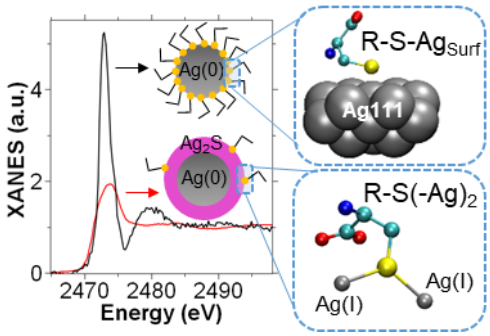
XANES (a.u.)
0
2
4
2470
2480
2490
Energy (eV)
Ag(0)
Ag2S
Ag(0)
R-S-AgSurf
Ag111
R-S(-Ag)2
Ag(I)
Ag(I)